Bnip3 and AIF cooperate to induce apoptosis and cavitation during epithelial morphogenesis

Yanmei Qi,[1] Xiaoxiang Tian,[1] Jie Liu,[1] Yaling Han,[2] Alan M. Graham,[1] M. Celeste Simon,[3] Josef M. Penninger,[4] Peter Carmeliet,[5] and Shaohua Li[1]

[1]Department of Surgery, University of Medicine and Dentistry New Jersey Robert Wood Johnson Medical School, New Brunswick, NJ 08093
[2]Shenyang Northern Hospital, Shenyang 110016, China
[3]Abramson Family Cancer Research Institute, University of Pennsylvania School of Medicine, Philadelphia, PA 19104
[4]Institute of Molecular Biotechnology of the Austrian Academy of Sciences, 1030 Vienna, Austria
[5]Vesalius Research Center, Vlaams Instituut voor Biotechnologie, Katholieke Universiteit Leuven, Leuven 3000, Belgium

Apoptosis is an essential step in cavitation during embryonic epithelial morphogenesis, but its mechanisms are largely unknown. In this paper, we used embryonic stem cell–differentiated embryoid bodies (EBs) as a model and found that Bnip3 (Bcl-2/adenovirus E1B 19-kD interacting protein), a BH3-only proapoptotic protein, was highly up-regulated during cavitation in a hypoxia-dependent manner. Short hairpin RNA silencing of Bnip3 inhibited apoptosis of the core cells and delayed cavitation. We show that the Bnip3 up-regulation was mediated mainly by hypoxia-inducible factor (HIF)–2. Ablation of HIF-2α or HIF-1β, the common β subunit of HIF-1 and -2, suppressed Bnip3 up-regulation and inhibited apoptosis and cavitation. We further show that apoptosis-inducing factor (AIF) cooperated with Bnip3 to promote lumen clearance. Bnip3 silencing in AIF-null EBs nearly blocked apoptosis and cavitation. Moreover, AIF also regulated Bnip3 expression through mitochondrial production of reactive oxygen species and consequent HIF-2α stabilization. These results uncover a mechanism of cavitation through hypoxia-induced apoptosis of the core cells mediated by HIFs, Bnip3, and AIF.

Introduction

Epithelial lumen formation is a fundamental process critical for early embryogenesis and development of tubular organs such as mammary gland, kidney, and lung. The lumen forms by one of the two mechanisms: invagination and fusion of an epithelial sheet or hollowing of a solid cell mass, which in turn is mediated by vacuolar exocytosis, directional fluid transport, membrane repulsion, and/or apoptosis-dependent cavitation (Hogan and Kolodziej, 2002; Datta et al., 2011). The latter contributes to the morphogenesis of mammary acini, salivary gland, ureteric buds, and the egg cylinder–stage embryo (Coucouvanis and Martin, 1995; Debnath et al., 2002; Meyer et al., 2004; Mailleux et al., 2007; Pradhan et al., 2010; Wells and Patel, 2010).

Embryoid bodies (EBs) differentiated from embryonic stem (ES) cells and embryocarcinoma cells have been used as a model to study the molecular mechanisms of cavitation during epithelial morphogenesis (Coucouvanis and Martin, 1995; Li et al., 2003). When grown in aggregate suspension culture, ES cells undergo compaction and form spherical EBs in 1–2 d. Apoptotic cells are sparsely distributed in EBs at this stage of differentiation (Li et al., 2002; He et al., 2010). Later, endoderm develops on the EB surface, which is followed by the assembly of an underlying basement membrane. Beginning on day 3, the epiblast cells in contact with the basement membrane polarize to form a pseudostratified columnar epiblast epithelium (CEE), which is characterized by the formation of an apical membrane domain separated from the basolateral membranes by adherens and tight junctions. At the same time, increased apoptosis of the inner nonpolar cells is observed in two distinct locations: one adjacent to the apex of the epiblast epithelium, which leads to the formation of slitlike clefts (peripheral apoptosis), and the other at the center of the EB, which proceeds outward (central apoptosis; He et al., 2010). In 5–7 d, all the core cells enclosed by the epiblast epithelium

Correspondence to Shaohua Li: shaohua.li@umdnj.edu

Abbreviations used in this paper: AIF, apoptosis-inducing factor; BMP, bone morphogenetic protein; CEE, columnar epiblast epithelium; ChIP, chromatin immunoprecipitation; DHE, dihydroethidium; EB, embryoid body; ES, embryonic stem; HIF, hypoxia-inducible factor; RIPA, radioimmunoprecipitation assay; ROS, reactive oxygen species; shRNA, short hairpin RNA.

The Rockefeller University Press $30.00
J. Cell Biol. Vol. 198 No. 1 103–114
www.jcb.org/cgi/doi/10.1083/jcb.201111063

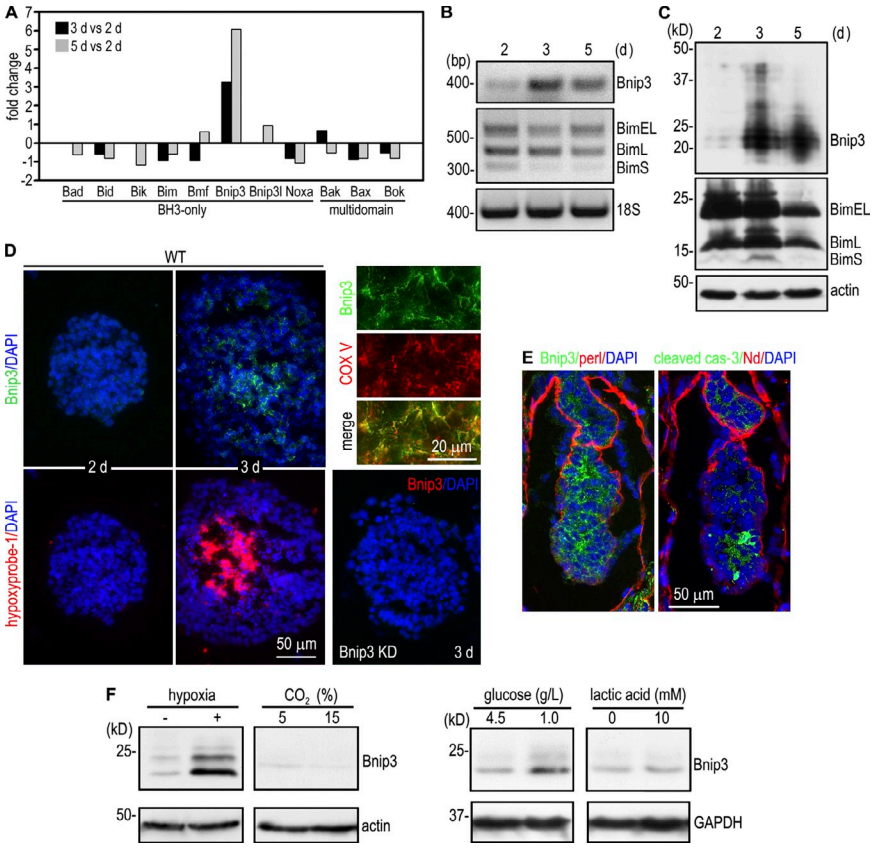

Figure 1. **Bnip3 is selectively up-regulated during embryonic epithelial morphogenesis.** (A) Microarray analysis of mRNAs for BH domain–containing proapoptotic proteins revealed selective up-regulation of Bnip3 during EB differentiation. The data shown are the mean of two detections. (B) RT-PCR analysis showed that the mRNA for Bnip3 but not Bim was increased during EB differentiation. (C) Normal EBs cultured for 2, 3, and 5 d were analyzed by immunoblotting for Bnip3 and Bim. Actin serves as a loading control. Bnip3 expression was significantly increased in 3- and 5-d EBs. (D) 2- and 3-d EBs were incubated with 10 μM hypoxyprobe-1 for 2 h and immunostained for Bnip3 and hypoxyprobe-1. A central hypoxic zone was evident in 3-d EBs. Bnip3 was mainly expressed in the cells in or near the hypoxic zone. Bnip3 knockdown (KD) EBs served as a negative control for Bnip3 staining. 3-d EBs were also costained for Bnip3 and the mitochondrial marker complex V (COX V). Bnip3 colocalized with complex V. (E) E5.0 mouse embryos were immunostained for Bnip3, cleaved caspase-3 (cas-3), and the basement membrane proteins perlecan (perl) and nidogen (Nd). (F) 1-d EBs were cultured at 37°C for 16 h under the following conditions: in hypoxic pouches (GasPak EZ; BD), under 5% (pH 7.2) or 15% CO_2 (pH 6.7), in media containing 4.5 g/L or 1.0 g/L glucose, and in media with (pH 6.7) or without (pH 7.2) 10 mM lactic acid. EBs were analyzed by immunoblotting for Bnip3, actin, and glyceraldehyde 3-phosphate dehydrogenase (GAPDH). Hypoxia significantly up-regulated Bnip3 expression, whereas low glucose led to a moderate increase.

are cleared by programmed cell death converged from these two sites, creating a proamniotic-like cavity.

A study using embryocarcinoma cell–derived EBs has indicated that a death signal produced by visceral endoderm induces the peripheral apoptosis and cleft formation (Coucouvanis and Martin, 1995). A further study has shown that bone morphogenetic protein (BMP)–2 is highly expressed in visceral endoderm and that expression of a dominant-negative BMP receptor in EBs blocked the apoptosis and cavitation, suggesting BMP-2 to be the death signal (Coucouvanis and Martin, 1999). Basement membrane is also thought to play a role in the cleft formation, as targeted deletion of the laminin γ1 gene prevents basement membrane formation and blocks the peripheral apoptosis (Murray and Edgar, 2000). However, the apoptosis initiated from the EB center still occurs in the absence of endoderm and basement membrane, and the mechanisms involved are unknown (Li et al., 2002; Liu et al., 2009).

In this study, we show that Bnip3 (Bcl-2/adenovirus E1B 19-kD interacting protein 3), a BH3-only proapoptotic protein, is markedly up-regulated in the core cells by hypoxia during EB differentiation. Short hairpin RNA (shRNA) silencing of Bnip3 inhibits apoptosis of the core cells and delays EB cavitation. We further show that hypoxia-inducible factor (HIF)–2α is selectively increased in the core cells in parallel with Bnip3, whose up-regulation is significantly attenuated in HIF-$2\alpha^{-/-}$ and HIF-$1\beta^{-/-}$ EBs. Lastly, we demonstrate that silencing of Bnip3 in apoptosis-inducing factor (AIF)–null EBs leads to additional inhibition of apoptosis and a blockade of cavitation. Altogether, our data provide evidence for a mechanism whereby HIF-dependent up-regulation of Bnip3 cooperates with AIF to promote cavitation and epithelial lumen formation by inducing apoptosis of the core cells.

Results

Bnip3 is selectively up-regulated in the core cells during EB morphogenesis

To seek the molecules implicated in apoptosis-mediated cavitation during embryonic epithelial morphogenesis, we determined the transcription profile of EBs at different stages of differentiation using Affymetrix GeneChip mouse whole-genome microarray. An analysis of proapoptotic genes revealed that Bnip3 was selectively up-regulated in 3-d EBs when cavitation was initiated and was further increased in 5-d EBs when cavitation was in rapid progression (Fig. 1 A; He et al., 2010). To confirm the microarray data, we examined the temporal expression of Bnip3 by RT-PCR and immunoblotting. Bnip3 mRNA was increased by 13 and 10 fold in 3- and 5-d EBs when compared with 2-d EBs. This corresponds to an 11- and eightfold increase of Bnip3 at the protein level (Fig. 1, B and C). In contrast, the expression of Bim, a BH3-only protein involved in apoptosis and cavitation of mammary acini, was reduced during EB morphogenesis (Mailleux et al., 2007). Bnip3 has been reported to be induced by hypoxia in both normal and transformed cells (Bruick, 2000). During morphogenesis, EB size increases significantly, reaching 50–100 μm in diameter by day 2 and 250–500 μm by day 3.

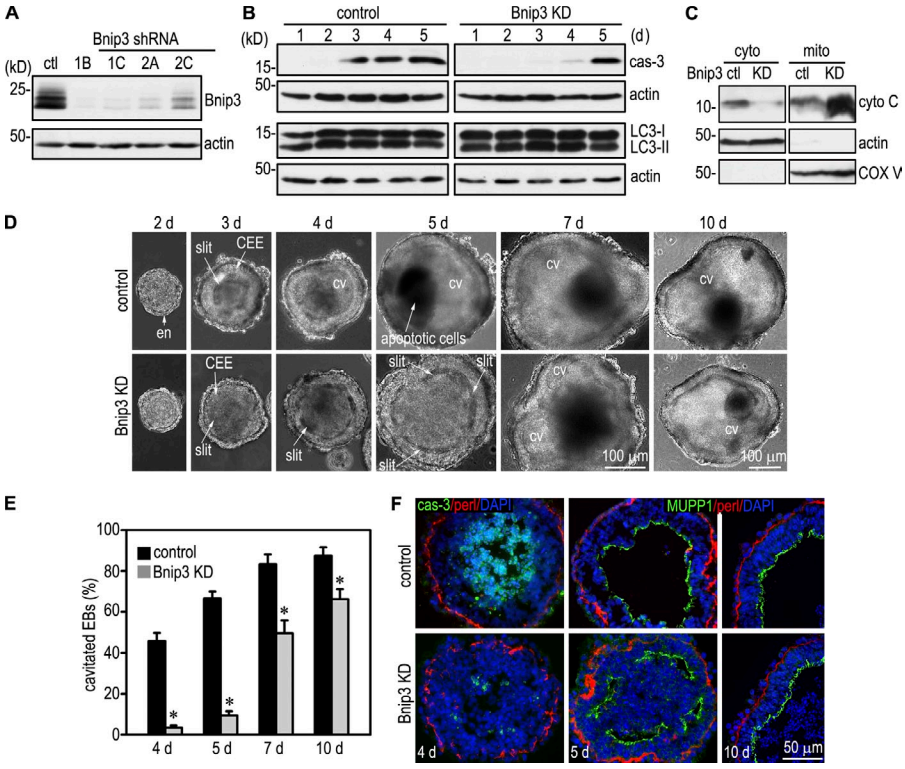

Figure 2. **Bnip3 knockdown inhibits apoptosis and cavitation.** (A) Stable ES cell clones expressing Bnip3 shRNAs or the scrambled control (ctl) were established based on puromycin resistance and GFP fluorescence. Immunoblot analysis of 3-d EBs showed a reduction of Bnip3 expression by 97% in clone 1B. (B) Bnip3 knockdown (KD; clone 1B) and control EBs were cultured for 1–5 d and analyzed by immunoblotting for cleaved caspase-3 (cas-3), microtubule-associated protein 1 LC3, and actin. Bnip3 knockdown inhibited caspase-3 activation but not the conversion of LC3-I to LC3-II. (C) Cytosolic (cyto) and mitochondrial (mito) preparations of 3-d control and Bnip3 knockdown EBs were analyzed by immunoblotting for cytochrome C (cyto C). Actin serves as a cytosolic loading control, and complex V (COX V) serves as a mitochondrial loading control. Bnip3 knockdown inhibited cytochrome C release from the mitochondria to the cytoplasm. (D) Live-phase micrographs show the differentiation of endoderm (en) and the CEE and the formation of a proamniotic-like cavity (CV). Bnip3 knockdown significantly delayed the clearance of centrally located cells. (E) EBs with a central cavity were counted by live-phase microscopy and plotted as a percentage of total EBs examined. $n = 7$ independent experiments with a total of 1,387–1,906 EBs for each group. Error bars represent the mean ± SD. *, $P < 0.01$. (F) EBs were cultured for 4, 5, and 10 d and immunostained for cleaved caspase-3, the apical polarity marker MUPP1, and basement membrane perlecan (perl). The nucleus was counterstained with DAPI. Bnip3 knockdown inhibited apoptosis and delayed lumen clearance but had no effect on epiblast polarity.

We reasoned that this increase in size may lead to hypoxia in the core cells. Our microarray analysis showed that transcription of many hypoxia-regulated genes was markedly increased together with Bnip3 (Fig. S1). To determine the spatial relationship between hypoxia and Bnip3 expression in EBs, we labeled the hypoxic zone in EBs with hypoxyprobe-1 (pimonidazole hydrochloride), which binds to cells and forms adducts under hypoxic conditions (Varghese et al., 1976; Arteel et al., 1995). Coimmunostaining for hypoxyprobe-1 and Bnip3 showed that hypoxyprobe-1 did not label 2-d EBs in which Bnip3 was barely detectable. In contrast, in ∼86% of 3-d EBs, hypxyprobe-1 clearly marked a central zone in which apoptotic cells could be identified by fragmented nuclei and cleaved caspase-3 staining (Fig. 1 D and not depicted). Bnip3 was highly expressed in the cells within and/or adjacent to the hypoxic zone and was colocalized with mitochondrial complex V. In embryonic day 5.0 (E5.0) mouse embryos, both Bnip3 and cleaved caspase-3 were detected in the centrally located cells before cavitation (Fig. 1 E). To test whether hypoxia induces Bnip3 in EBs, we cultured 1-d EBs in hypoxia pouches for 16 h and found that the Bnip3 protein level was significantly up-regulated (Fig. 1 F). In addition to hypoxia, there are gradients for glucose, lactate, and pH in differentiating EBs. However, our experiments showed that Bnip3 expression was not significantly affected by pH alterations or lactic acidosis (Fig. 1 F). A reduction in glucose concentrations moderately increased Bnip3 expression. Collectively, these results suggest that Bnip3 is selectively up-regulated during EB morphogenesis mainly as a result of reduced oxygen availability in the interior of EBs.

Silencing of Bnip3 inhibits apoptosis of the core cells and delays cavitation

To elucidate the role of Bnip3 in EB morphogenesis, we established 12 ES cell clones that stably expressed four distinct shRNAs targeting mouse Bnip3. Immunoblotting showed that in clone 1B, Bnip3 expression was reduced by 97% at the protein level when compared with the scrambled control (Fig. 2 A). shRNA-mediated Bnip3 silencing inhibited caspase-dependent apoptosis in the early stage of EB differentiation, particularly during days 3 and 4 when cavitation was in rapid progression (Fig. 2 B). Bnip3 can also induce autophagy in response to cellular stresses (Daido et al., 2004; Zhang and Ney, 2009), and autophagy has been suggested to contribute to the removal of apoptotic cells during EB cavitation (Qu et al., 2007). To test whether Bnip3 regulates autophagy in EBs, we analyzed the conversion of microtubule-associated protein light chain 3-I (LC3-I) to LC3-II, which correlates with the number of autophagosomes (Mizushima and Yoshimori, 2007). Immunoblotting revealed no significant difference in the ratio of LC3-I to LC3-II between Bnip3 knockdown and control EBs (Fig. 2 B). In addition, the ratio was unchanged

during EB morphogenesis. Immunostaining showed that LC3 was expressed in the centrally located cells in a punctuate pattern, but again, no difference was observed between Bnip3 knockdown and control EBs (unpublished data). Overexpression of Bnip3 in fibroblasts or treatment of isolated mitochondria with recombinant Bnip3 could induce mitochondrial membrane permeability and cytochrome C release (Kubli et al., 2007; Quinsay et al., 2010). Cytochrome C released into the cytoplasm can activate caspases and trigger the intrinsic apoptosis pathway (Green and Reed, 1998). To test whether Bnip3 knockdown inhibits cytochrome C release, we performed immunoblot analysis of cytosolic and mitochondrial preparations. Silencing of Bnip3 decreased cytosolic and increased mitochondrial cytochrome C levels (Fig. 2 C). These results suggest that Bnip3 mediates apoptosis but not autophagy during EB differentiation, likely through inducing cytochrome C release from mitochondria.

To assess the effect of Bnip3 silencing on EB cavitation, we cultured EBs for 2–10 d and quantified the percentage of EBs with a central cavity by live-phase microscopy. As shown in Fig. 2 (D and E), control EBs cultured for 3 d formed slits between the apex of the CEE and the remaining inner cells. Apoptosis was detected in these slits by cleaved caspase-3 staining (He et al., 2010). By 4 d, nearly half of the control EBs developed a central cavity, and cavitated EBs reached 67% by 5 d. In contrast, most of the Bnip3 knockdown EBs still remained at the slit stage on day 5, and only some small EBs displayed a central cavity. After 7 and 10 d, cavitation of Bnip3 knockdown EBs speeded up, but the efficiency was still lower than the controls. Immunostaining for cleaved caspase-3 showed massive apoptosis of the centrally located cells in 4-d control EBs, whereas only scattered cells were positively stained in the slits in Bnip3 knockdown EBs (Fig. 2 F). Altogether, these results show that Bnip3 induces apoptosis and promotes the formation of epithelial cysts during EB morphogenesis. Bnip3 silencing causes a significant delay in cavitation.

Next, we tested whether Bnip3 knockdown affects epiblast polarity. 5-d EBs were immunostained for the apical polarity marker MUPP1, and the apical actin belt was visualized with rhodamine-phalloidin. Bnip3 silencing inhibited apoptosis-dependent removal of the core cells in 5-d EBs and led to the formation of multiple peripheral slits and/or small cavities (Fig. 2 F). However, MUPP1 and F-actin were localized to the apex of epiblast cells (Fig. 2 F and not depicted). The basement membrane receptors integrin β1 and dystroglycan were also correctly targeted to the basal side of epiblast (unpublished data). By 10 d, these small cavities had fused into a central cavity. These results indicate that Bnip3 is not required for epiblast polarization.

HIFs are required for Bnip3 up-regulation and apoptosis

HIFs are key regulators of cellular responses to hypoxia (Majmundar et al., 2010). To determine the role of HIFs in Bnip3 up-regulation during EB morphogenesis, we examined the temporal expression of HIF-1α, HIF-2α, and HIF-1β (aryl hydrocarbon receptor nuclear translocator) by immunoblotting. HIF-1α was hardly detectable during 5 d of EB differentiation, whereas HIF-2α was significantly increased on day 3 and remained high thereafter in parallel to Bnip3 (Fig. 3, A and F). As expected, HIF-1β was constitutively expressed. Importantly, immunostaining demonstrated that HIF-2α was selectively expressed in the nucleus of the centrally located cells (Fig. 3 E). In contrast, HIF-1β was detected in the nucleus of all the cells. Immunoprecipitation of nuclear preparations of 3-d normal EBs revealed that HIF-2α bound to HIF-1β, suggesting that they form a transcription complex in the nucleus (Fig. 3 D). Given that the mRNAs for HIF-1α and HIF-2α were unchanged during EB morphogenesis, as assessed by microarray analysis (unpublished data), these results support the notion that the HIF-2α protein is selectively stabilized under chronic hypoxia in the core cells of differentiating EBs.

In undifferentiated mouse ES cells, the activation of hypoxia-responsive genes is mainly mediated by HIF-1, whereas HIF-2 is transcriptionally inactive, although both HIF-1α and HIF-2α are increased at the protein level under acute hypoxic conditions (Hu et al., 2003). In addition, targeted disruption of HIF-1α but not HIF-2α inhibits hypoxia-induced ES cell apoptosis (Carmeliet et al., 1998; Brusselmans et al., 2001). To determine the role of HIFs in the up-regulation of Bnip3 and apoptosis and the contribution of individual α subunits, we compared EBs differentiated from wild-type, HIF-1α, HIF-2α, and HIF-1β$^{-/-}$ ES cells. The loss of HIF-1α and -2α in the corresponding null mutant EBs was confirmed by immunoblot analysis of 1-d EBs cultured in hypoxia for 16 h (Fig. 3 B). Time-course experiments showed that Bnip3 expression increased significantly on day 3 and remained at high levels on days 4 and 5 in wild-type EBs (Fig. 3 F). The level of Bnip3 expression correlated well with that of cleaved caspase-3. Ablation of HIF-1α slightly attenuated Bnip3 up-regulation on day 3 but not on days 4 and 5, suggesting that HIF-1α partially contributes to the early induction of Bnip3. In contrast, Bnip3 up-regulation was significantly inhibited in HIF-2α$^{-/-}$ and HIF-1β$^{-/-}$ EBs. It is worth pointing out that long exposure of the blots revealed low levels of Bnip3 expression in HIF-1β$^{-/-}$ EBs, suggesting that Bnip3 expression is not entirely dependent on HIFs. A previous study has indicated that Bnip3 is a unique HIF-1–responsive gene. Overexpression of HIF-1α but not HIF-2α in HEK293 cells up-regulates Bnip3 expression (Wang et al., 2005). Our results suggest that in chronic hypoxia, HIF-2α can also mediate Bnip3 up-regulation. The suppression of Bnip3 in HIF-2α$^{-/-}$ and HIF-1β$^{-/-}$ EBs was accompanied by a marked reduction of cleaved casplase-3, suggesting that HIFs are responsible for the induction of apoptosis during EB morphogenesis.

The promoter of the mouse Bnip3 gene contains a hypoxia-responsive element. To determine whether HIF-2 binds to the Bnip3 promoter, we performed chromatin immunoprecipitation (ChIP) on 3-d EBs using anti–HIF-2α antibody. The Bnip3 promoter sequence was immunoprecipitated in normal but not HIF-2α$^{-/-}$ EBs, suggesting that the PCR product generated from HIF-2α immunoprecipitates was specific (Fig. 3 G). We also performed ChIP assay for

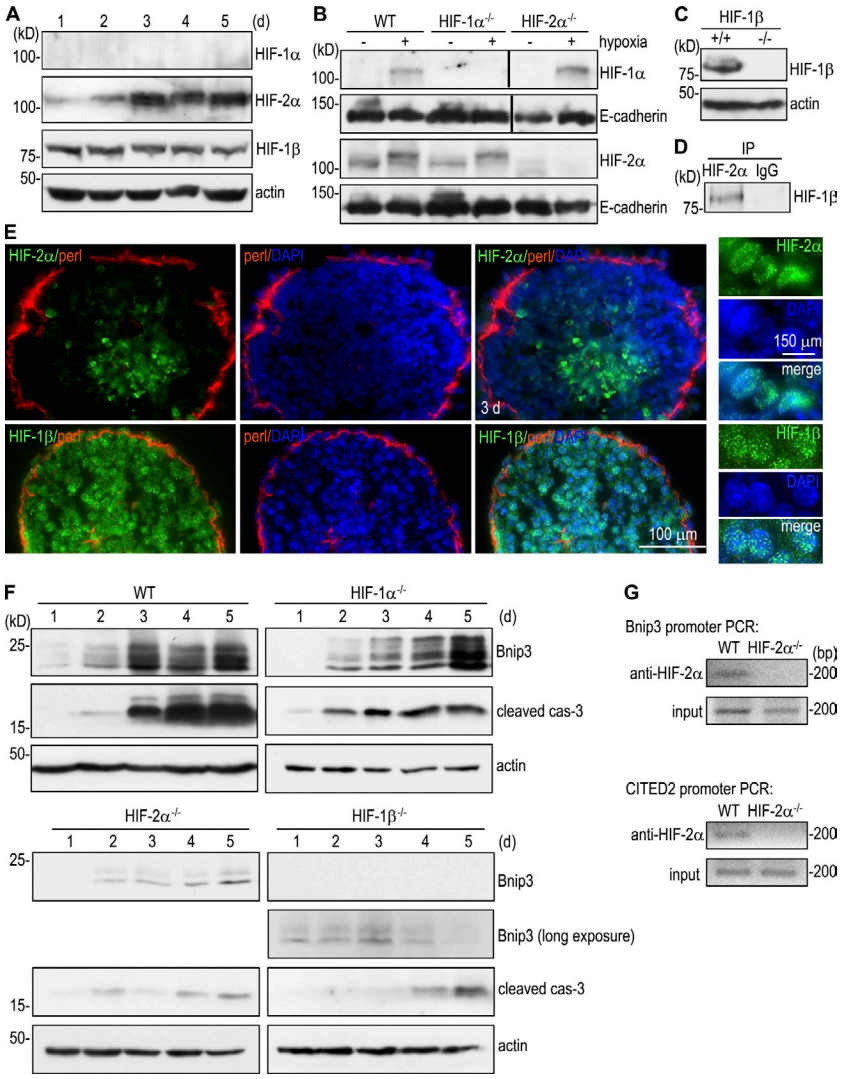

Figure 3. **HIFs mediate Bnip3 up-regulation and apoptosis.** (A) Immunoblot analysis of normal EBs cultured for 1–5 d showed that HIF-2α was selectively up-regulated during EB differentiation. (B) 1-d EBs were cultured in hypoxic pouches for 16 h and then analyzed by immunoblotting for HIF-1α and -2α. HIF-1α and -2α were absent from HIF-1α$^{-/-}$ and HIF-2α$^{-/-}$ EBs, respectively. Black lines indicate that intervening lanes have been spliced out. WT, wild type. (C) Immunoblots show that HIF-1β was not expressed in HIF-1β$^{-/-}$ EBs. (D) Nuclear lysates of 3-d normal EBs were immunoprecipitated (IP) with HIF-2α antibody or control IgG followed by immunoblotting for HIF-1β. HIF-2α coimmunoprecipitated with HIF-1β. (E) Immunostaining showed that HIF-2α was localized to the nucleus of the core cells of 3-d EBs, whereas HIF-1β was detected in the nucleus of all cells. perl, perlecan. (F) EBs were cultured for 1–5 d and analyzed for Bnip3 and cleaved caspase-3 (cas-3) by immunoblotting. Bnip3 was significantly up-regulated during EB differentiation in wild-type and HIF-1α$^{-/-}$ EBs but was only minimally induced in HIF-2α$^{-/-}$ and HIF-1β$^{-/-}$ EBs. The level of cleaved caspase-3 correlated with that of Bnip3. (G) ChIP of HIF-2α interactions with the Bnip3 and CITED2 promoters. Bands are PCR products targeting −308 to −101 of the Bnip3 promoter and −1,512 to −1,329 of CITED2 promoter. HIF-2α specifically interacted with the Bnip3 promoter. CITED2 ChIP was used as a positive control.

HIF-2α binding to the promoter of CITED2, a known HIF-2α target gene, as a positive control and obtained a similar result. These results suggest that HIF-2α directly binds to the Bnip3 promoter and transactivates its expression.

HIFs promote apoptosis and cavitation through Bnip3

Because HIFs induce Bnip3 up-regulation and apoptosis, we reasoned that HIFs might also facilitate cavitation during EB morphogenesis. To test this, we compared the differentiation of normal EBs with those deficient for HIF-1β, the common β subunit for HIF-1α and -2α. Similar to Bnip3 knockdown EBs, HIF-1β$^{-/-}$ EBs could differentiate to form endoderm and polarized epiblast, but cavitation was delayed (Fig. 4, A–C). After 5 d in culture, >50% of normal EBs formed a central cavity, which often contains residual apoptotic cells and debris, whereas most of the HIF-1β$^{-/-}$ EBs only developed clefts between the apex of the CEE and the remaining core cells. Central apoptosis rarely occurred in the mutant EBs. Cavitation (<20% of the mutant EBs) was observed mostly in small EBs, which is less dependent on apoptosis. After 10 d, cavitation efficiency of the mutant EBs was significantly increased but still less than the normal control. These results suggest that HIFs induce apoptosis of the core cells and promote cavitation during EB morphogenesis.

To determine whether Bnip3 mediates HIF-1β–dependent apoptosis of the core cells and cavitation, we stably overexpressed Bnip3 in HIF-1β$^{-/-}$ EBs (Fig. 4 D). Compared with normal and HIF-1β$^{-/-}$ EBs transfected with the control vector, overexpression of Bnip3 in HIF-1β$^{-/-}$ EBs increased apoptosis, as indicated by elevated cleaved caspase-3 levels. Consequently, the cavitation process was accelerated compared with HIF-1β$^{-/-}$ EBs transfected with the control vector (Fig. 4 E). Bnip3 overexpression promoted apoptosis of the core cells (Fig. 4 F). In addition, the basement membrane–contacting epiblast cells, which are normally protected by anchorage-dependent survival factors (Coucouvanis and Martin, 1995; He et al., 2010), were often observed to undergo apoptosis. Similarly, we also stably overexpressed Bnip3 in HIF-2α$^{-/-}$ EBs and observed markedly increased apoptosis compared with HIF-2α$^{-/-}$ EBs expressing GFP alone (Fig. 4 G). This was accompanied by accelerated cavitation on days 4, 5, and 7 of culturing (Fig. 4 H). Collectively, these results suggest that HIFs promote apoptosis and cavitation through Bnip3 during EB morphogenesis.

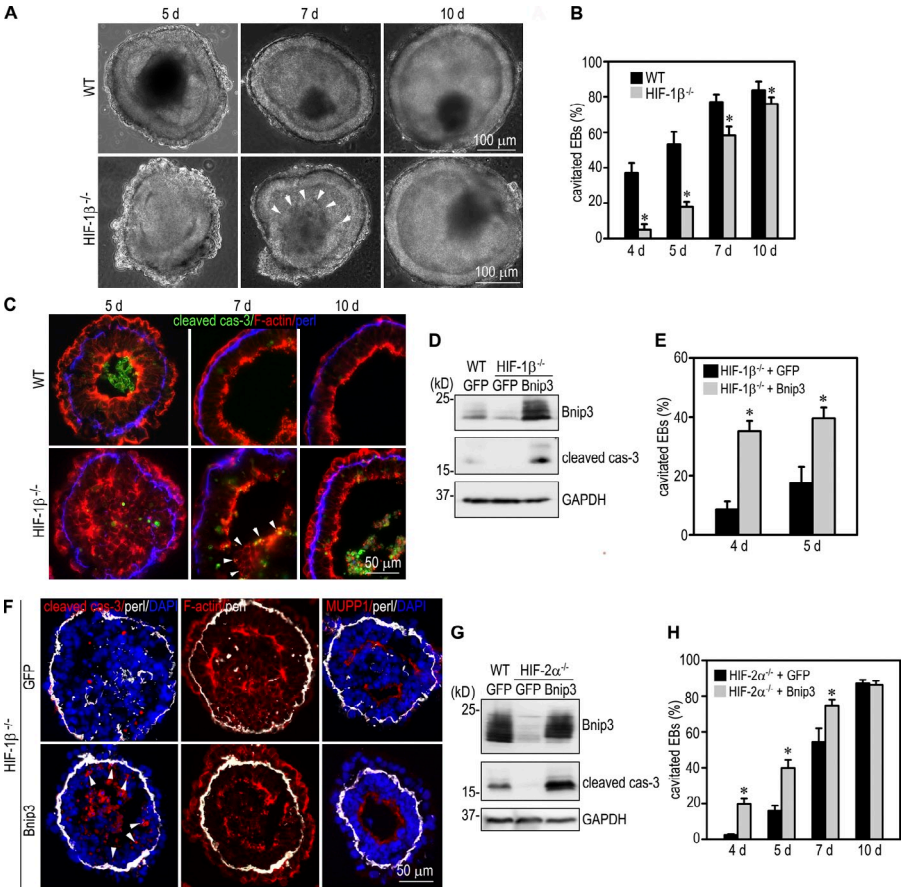

Figure 4. **HIFs promote cavitation through Bnip3.** (A) Live-phase micrographs show a delay in cavitation in HIF-1β$^{-/-}$ EBs. Arrowheads indicate the remaining core of a 7-d mutant EB. WT, wild type. (B) EBs with a central cavity were counted and plotted as a percentage of total EBs examined. *n* = 10 independent experiments with a total of 856–932 EBs for each group. Error bars represent the mean ± SD. *, P < 0.01. (C) Immunostaining for cleaved caspase-3 (cas-3) revealed reduced central apoptosis in 5-d HIF-1β$^{-/-}$ EBs. Arrowheads indicate the remaining core of a 7-d mutant EB. perl, perlecan. (D) Wild-type EBs stably transfected with GFP and HIF-1β$^{-/-}$ EBs transfected with Bnip3 or GFP were cultured for 2 d and subjected to immunoblotting for Bnip3 and cleaved caspase-3. Glyceraldehyde 3-phosphate dehydrogenase (GAPDH) serves as a loading control. Overexpression of Bnip3 increased apoptosis in HIF-1β$^{-/-}$ EBs. (E) HIF-1β$^{-/-}$ EBs transfected with Bnip3 or GFP were cultured for 4 and 5 d and examined by live-phase microscopy. The percentage of EBs with a central cavity was plotted. *n* = 8 independent experiments with a total of 952–1,114 EBs for each group. Error bars represent the mean ± SD. *, P < 0.01. (F) 5-d EBs were immunostained for cleaved caspase-3, MUPP1, and perlecan. F-actin was stained with rhodamine-phalloidin. Overexpression of Bnip3 in HIF-1β$^{-/-}$ EBs promoted central apoptosis and cavitation. It also caused apoptosis of the epiblast cells in contact with the basement membrane (arrowheads). (G) Wild-type GFP EBs and HIF-2α$^{-/-}$ EBs transfected with Bnip3 or GFP were cultured for 3 d and subjected to immunoblotting for Bnip3 and cleaved caspase-3. Overexpression of Bnip3 increased apoptosis in HIF-2α$^{-/-}$ EBs. (H) The cavitation efficiency of HIF-2α$^{-/-}$ EBs expressing Bnip3 or GFP was counted and plotted. *n* = 9–23 independent experiments with a total of 900–2,270 EBs for each group. Error bars represent the mean ± SD. *, P < 0.01.

Bnip3 cooperates with AIF to induce apoptosis and cavitation

Bnip3-null mice are born and fertile, suggesting that other factors also contribute to apoptosis and cavitation in the early embryo (Diwan et al., 2007). To determine whether Bnip3 fulfills the task in combination with other proapoptotic proteins, we examined the role of Bim and AIF, two mitochondrial death–inducing factors highly expressed in early embryos and differentiating EBs. In contrast to silencing of Bnip3, knockdown of Bim had no effect on apoptosis and cavitation (Fig. S2 [C and E] and not depicted). Furthermore, combined knockdown of Bnip3 and Bim in EBs did not further inhibit cavitation (Fig. S2, D and E), suggesting that Bim is not involved in EB apoptosis and cavitation.

A previous study has demonstrated that AIF induces apoptosis in many cell types and is believed to act in a caspase-independent manner (Modjtahedi et al., 2006). Genetic studies in mice revealed that AIF is required for embryogenesis, and its inactivation inhibits apoptosis, although a different strategy of gene targeting showed that AIF-null EBs could cavitate (Joza et al., 2001; Brown et al., 2006). To clarify the role of AIF in apoptosis and cavitation, we analyzed EBs differentiated from AIF$^{y/+}$ and AIF$^{y/-}$ (AIF is encoded by a single gene located on the X chromosome) ES cells generated using a conventional targeting strategy (Joza et al., 2001; Brown et al., 2006). Time-course experiments showed a significant elevation of caspase-3 activation in 3- and 4-d AIF$^{y/+}$ EBs but only a moderate increase in 4-d AIF$^{y/-}$ EBs (Fig. 5 B). We counted EBs with a central cavity by phase microscopy and observed a significant delay in cavitation (Fig. 5, C, D, and F). After 4 d, 41% of the AIF$^{y/+}$ EBs formed a central cavity, whereas only 2% of AIF$^{y/-}$ EBs cavitated. By 7 d, the cavitation efficiency of AIF$^{y/+}$ EBs was still twice that of AIF$^{y/-}$ EBs (84% vs. 39%), although the cavitation efficiency of the null EBs was close to normal in 10-d EBs. Immunostaining of 4- and 5-d EBs with anti–cleaved caspase-3 and anti-MUPP1 antibodies demonstrated normal epiblast polarity despite reduced apoptosis and lumen clearance in AIF$^{y/-}$ EBs (Fig. 5 D). To test whether AIF cooperates with Bnip3 to mediate EB cavitation, we suppressed Bnip3 expression in AIF$^{y/-}$ EBs by stable shRNA transfection. Immunoblot analysis of 5-d EBs showed that silencing of Bnip3 in the AIF-null background further reduced caspase-3 activation (Fig. 5 E). Consequently, cavitation of the EBs was

significantly inhibited compared with AIF$^{y/-}$ and Bnip3 knockdown EBs (Figs. 2 E and 5 F). Altogether, these results suggest that Bnip3 and AIF cooperate to induce apoptosis and cavitation during EB morphogenesis.

AIF regulates Bnip3 expression through HIFs

To investigate the mechanisms through which AIF induces apoptosis, we first immunostained 4-d EBs containing a central apoptotic zone with anti-AIF antibody. Strong AIF expression was detected in a punctate pattern in endoderm and polarized epiblast as well as the core cells undergoing apoptosis (Fig. 6 A). AIF colocalized with mitochondrial complex V in both live and dying cells. We were unable to detect AIF in the nucleus of the apoptotic cells. A similar distribution of AIF was also observed in E5.0 mouse embryos (Fig. 6 B). This spatial expression pattern indicates that apoptosis induced by AIF during EB morphogenesis is not caused by AIF translocation to the cytoplasm and then to the nucleus, as previously suggested (Susin et al., 1999). AIF is a flavoprotein critical for the normal function of mitochondria, which not only act as the cell's powerhouse but also as an oxygen sensor in hypoxia. To determine whether AIF induces apoptosis at least partly through Bnip3, we analyzed AIF$^{y/+}$ and AIF$^{y/-}$ EBs cultured for 3–5 d when Bnip3 is significantly up-regulated. Immunoblotting showed that Bnip3 was expressed in AIF$^{y/-}$ EBs at much lower levels compared with AIF$^{y/+}$ EBs (Fig. 6 C), suggesting that AIF regulates Bnip3 expression. The reduced Bnip3 expression in AIF$^{y/-}$ EBs corresponded to a 90% reduction of HIF-2α (Fig. 6, D and E). Treatment of normal EBs with the mitochondrial complex I inhibitor rotenone also reduced expression of HIF-1/2α, Bnip3, and cleaved caspase-3 (Fig. 6 F). These data suggest that loss of AIF in the mitochondria impairs oxygen-sensing function, reduces HIF-α stability, and thereby inhibits hypoxia-induced Bnip3 up-regulation. To test this hypothesis, we stably expressed in AIF$^{y/-}$ EBs mutant HIF-1α PP (P402A and P564A) or HIF-2α PPN (P405A, P531A, and N847Q) that are stable under normoxia but still bind to DNA and activate transcription. Expression of either HIF-1α PP (clones C3 and C5) or HIF-2α PPN markedly increased Bnip3 expression compared with control EBs expressing GFP (Fig. 6, G and H). Collectively, these results suggest that AIF-induced apoptosis is partly mediated by HIF-2–dependent Bnip3 expression.

To determine whether AIF itself is regulated by hypoxia during EB differentiation, we performed immunoblotting on normal EBs cultured for 1–5 d. We observed no change in AIF expression over time during EB differentiation (Fig. S3 A). In line with this result, the AIF level was not altered in EBs cultured in hypoxia (Fig. S3 B). We also compared the AIF level of 4-d normal EBs with those null for HIF-1α, HIF-2α, or HIF-1β and found no difference among them (Fig. S3 C). These results suggest that AIF is not regulated by hypoxia per se but is permissive to hypoxia-induced HIF-2α stabilization and Bnip3 expression.

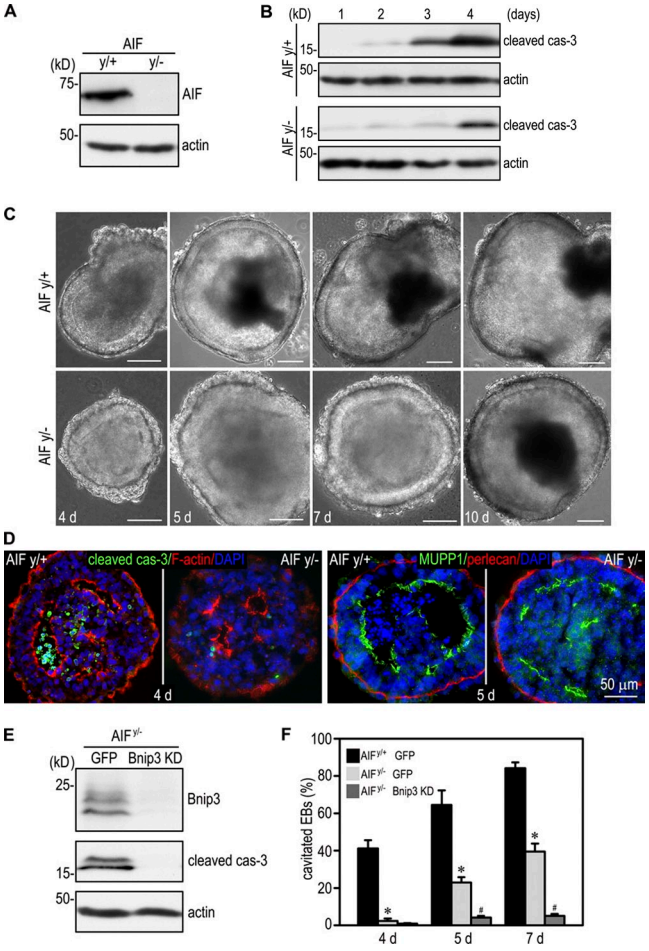

Figure 5. **Bnip3 cooperates with AIF to induce apoptosis and cavitation.** (A) 4-d AIF$^{y/+}$ and AIF$^{y/-}$ EBs were analyzed by immunoblotting for AIF. Actin was used as a loading control. (B) EBs were cultured for 1–4 d and analyzed by immunoblotting for cleaved caspase-3 (cas-3) and actin. Ablation of AIF inhibited caspase-3 activation. The 3 and 4 d actin data are the same as those in Fig. 6 C, where the same blots were analyzed for Bnip3 levels. (C) Live-phase micrographs show cavitation delay in AIF$^{y/-}$ EBs cultured for 4, 5, and 7 d. After 10 d, most of the AIF$^{y/-}$ EBs were cavitated similar to AIF$^{y/+}$ EBs. Bars, 100 μm. (D) 4-d EBs were immunostained for cleaved caspase-3. F-actin was stained with rhodamine-phalloidin to show the apical actin belt. Ablation of AIF inhibited apoptosis of the core cells. 5-d EBs were immunostained for the apical marker MUPP1. Apical polarization of the AIF$^{y/-}$ epiblast was not affected despite delayed lumen clearance. (E) AIF$^{y/-}$ ES cells were stably transfected with Bnip3 shRNA (Bnip3 knockdown [KD]) or GFP. 5-d EBs were analyzed by immunoblotting for Bnip3 and cleaved caspase-3. Bnip3 silencing in AIF$^{y/-}$ EBs further inhibited caspase-3 activation. (F) AIF$^{y/+}$ EBs expressing GFP and AIF$^{y/-}$ EBs stably transfected with Bnip3 shRNA or GFP were cultured for 4, 5, and 7 d. EB cavitation was quantitated by phase microscopy. EB cavitation was significantly delayed in the absence of AIF. Knockdown of Bnip3 in AIF$^{y/-}$ EBs nearly blocked cavitation. $n = 6$ independent experiments with a total of 529–808 EBs counted for each group. Error bars represent the mean ± SD. *, $P < 0.01$ versus AIF$^{y/+}$ GFP; #, $P < 0.01$ versus AIF$^{y/-}$ GFP.

Reactive oxygen species (ROS) mediate AIF-dependent HIF-2α stability, Bnip3 up-regulation, apoptosis, and cavitation

ROS produced in mitochondria has been shown to participate in oxygen sensing under hypoxic conditions (Brunelle et al., 2005; Guzy et al., 2005). To examine whether ROS production is changed in the absence of AIF, we incubated 3- and 4-d EBs with the fluorescent indicator dihydroethidium (DHE),

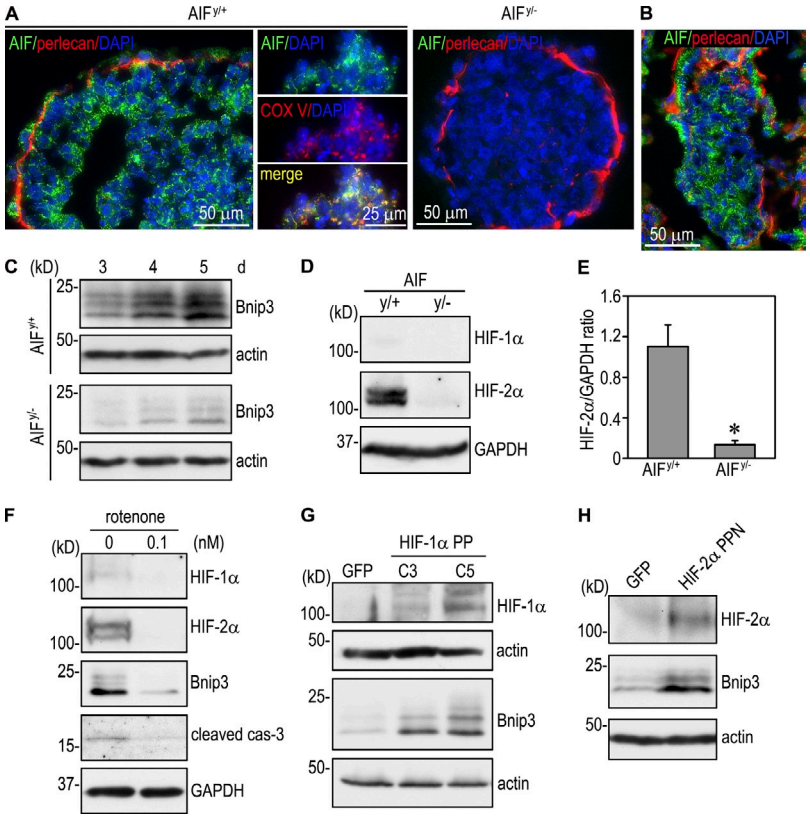

Figure 6. **Mitochondrial AIF regulates Bnip3 expression by stabilizing HIF-α.** (A) 4-d AIF$^{y/+}$ and AIF$^{y/-}$ EBs were stained for AIF and basement membrane perlecan. Nuclei were counterstained with DAPI. AIF was expressed in a punctate pattern in both polarized epiblast cells and core cells. AIF was not observed in the nucleus of the core cells undergoing apoptosis. The middle images show costaining of the core cells for AIF and mitochondrial complex V (COX V) in AIF$^{y/+}$ EBs. AIF colocalized with complex V. AIF$^{y/-}$ EBs were used as a negative control for AIF staining. (B) E5.0 embryos were immunostained for AIF and perlecan. AIF was expressed in both endoderm and epiblast. (C) AIF$^{y/+}$ and AIF$^{y/-}$ EBs were cultured for 3–5 d and analyzed for Bnip3 by immunoblotting. Bnip3 expression was significantly reduced in the absence of AIF. The 3 and 4 d actin data are the same as those in Fig. 5 B, where the same blots were analyzed for cleaved cas-3 levels. (D) Immunoblots show that the level of HIF-2α was much lower in 3-d AIF$^{y/-}$ EBs than in AIF$^{y/+}$ EBs. GAPDH, glyceraldehyde 3-phosphate dehydrogenase. (E) The blots were analyzed by densitometry, and the ratio of HIF-2α to glyceraldehyde 3-phosphate dehydrogenase was plotted. $n = 4$. Error bars represent the mean ± SD. *, $P < 0.01$. (F) Normal EBs were cultured in the presence or absence of 0.1 nM of the mitochondria complex I inhibitor rotenone for 3 d. Immunoblots show that rotenone treatment reduced the expression of HIF-1α, HIF-2α, Bnip3, and cleaved caspase-3 (cas-3). (G) AIF$^{y/-}$ EBs were stably transfected with GFP or mutant HIF-1α PP that is stable under normoxia but still binds to DNA and activates transcription. Expression of HIF-1α PP (clones C3 and C5) increased Bnip3 levels. (H) Immunoblots show that AIF$^{y/-}$ EBs stably expressing mutant HIF-2α PPN that is stable in normoxia led to Bnip3 up-regulation compared with the EBs expressing GFP. Actin serves as a loading control.

which emits red fluorescence after being oxidized by ROS. As shown in Fig. 7 A, ROS production was detected at the center of 3- and 4-d AIF$^{y/+}$ EBs and was significantly reduced in AIF$^{y/-}$ EBs. Incubation of 2-d AIF$^{y/-}$ EBs with 0.1 mM H_2O_2 for 24 h increased levels of HIF-2α, Bnip3, and cleaved caspase-3 (Fig. 7 B). In agreement with these findings, treatment of AIF$^{y/+}$ EBs with the ROS scavenger EUK134 reduced HIF-2α, Bnip3, and cleaved caspase-3 (Fig. 7 C). When 2-d EBs were incubated with 2 μM EUK134 for 5 d, cavitation was also significantly inhibited (Fig. 7 D). Surprisingly, we observed further inhibition of cavitation in Bnip3 knockdown EBs treated with EUK134, suggesting that ROS can promote cavitation independently of Bnip3. To test whether this is mediated by caspase activation, we treated 2-d Bnip3 knockdown EBs with 0.1 mM H_2O_2 for 24 h. H_2O_2 treatment only slightly increased cleaved caspase-3. We also incubated 1-d normal and HIF-1β$^{-/-}$ EBs with 0.1 mM H_2O_2 for 3 d. H_2O_2 treatment caused a small increase in the cavitation efficiency of both normal and HIF-1β$^{-/-}$ EBs (Fig. 7 F). Collectively, our results support a hypothesis that reduced oxygen availability to EB core cells stimulates ROS production in an AIF-dependent manner. In turn, ROS stabilizes HIF-α, which translocates to the nucleus and combines with HIF-1β to activate Bnip3 transcription. Bnip3 induces apoptosis of the core cells. ROS can also induce apoptosis and cavitation independently of HIFs and Bnip3 (Fig. 7 F). In addition, glucose reduction also contributes to Bnip3 elevation through HIFs because low glucose concentration moderately induced Bnip3 expression in normal but not HIF-1β$^{-/-}$ EBs (Figs. 1 F and S4).

Discussion

Cells in the center of a solid tissue primordium are usually limited by oxygen availability. However, the role of hypoxia in tissue morphogenesis has not been explored. In this study, we provide evidence that Bnip3 is up-regulated by hypoxia in the core cells of EBs and cooperates with AIF to induce apoptosis and cavitation in an HIF-dependent manner. Our data suggest a model in which hypoxia selectively stabilizes HIF-2α in the core cells via mitochondrial ROS production. HIF-2α translocates to the nucleus and dimerizes with constitutively expressed HIF-1β to activate Bnip3 transcription. AIF is also implicated in the regulation of ROS production, HIF-2α stabilization, and Bnip3 expression. In turn, Bnip3 induces apoptosis of the core cells and cavitation in cooperation with AIF.

AIF is a proapoptotic protein present in the intermembrane space of mitochondria and is released to the cytoplasm in response to death stimuli. The AIF gene is localized to the X chromosome. Targeted mutation of the AIF gene in ES cells failed to form chimeric mice after injected into host blastocysts (Joza et al., 2001). EBs cultured from AIF$^{y/-}$ ES cells had significantly reduced cell death and were unable to cavitate. Later, AIF was inactivated by crossing mice with a floxed AIF locus with mice expressing a β-actin *Cre* transgene (Joza et al., 2005; Brown et al., 2006). This approach revealed that AIF was not essential for EB cavitation and the formation of the proamniotic cavity. These studies suggest that proapoptotic proteins other than AIF or in combination with AIF may be required for apoptosis-dependent cavitation of the early embryo. In the present study, we showed that the BH3-only proapoptotic protein Bnip3

is selectively up-regulated at both mRNA and protein levels during EB differentiation and is localized in the hypoxic core cells. shRNA-mediated silencing of Bnip3 inhibits apoptosis and delays cavitation. Moreover, knockdown of Bnip3 expression in the AIF-null background further decreases apoptosis and nearly blocks EB cavitation. These data suggest that Bnip3 cooperates with AIF to induce apoptosis and cavitation during embryonic epithelial morphogenesis. Bim, another BH3-only protein highly expressed in early embryos and differentiating EBs, has been shown to induce apoptosis of mammary gland cells and contribute to cavitation-mediated acinar morphogenesis (Reginato et al., 2005; Mailleux et al., 2007). However, it is not involved in EB cavitation because Bim silencing does not promote apoptosis of the core cells. Furthermore, knockdown of both Bim and Bnip3 has no additive/synergistic effects on EB cavitation.

A previous study in various cultured cells has demonstrated that Bnip3 is a hypoxia-responsive gene regulated by HIF-1 (Chinnadurai et al., 2008). During EB morphogenesis, however, we detected very low levels of HIF-1α expression by immunoblotting, although HIF-1α, HIF-2α, and HIF-1β are similar at the mRNA level (unpublished data). In contrast, the HIF-2α protein is increased considerably over time and localized to the nucleus of the hypoxic core cells, closely correlating with the expression of Bnip3 and cleaved caspase-3. Importantly, genetic ablation of either HIF-2α or HIF-1β inhibited Bnip3 up-regulation and apoptosis. These results indicate that HIF-2α is selectively stabilized in the core cells during EB cavitation and is mainly responsible for Bnip3 induction. The stabilization of HIF-2α is likely a result of a gradual reduction of oxygen availability (chronic hypoxia) to the core cells as the size of EBs increases during differentiation. On the other hand, HIF-1α is preferably stabilized under acute hypoxic conditions (Holmquist-Mengelbier et al., 2006). We could also consistently detect elevated HIF-1α protein expression in EBs cultured overnight in hypoxia pouches. Under this condition, hypoxia-induced Bnip3 expression is inhibited by ablation of HIF-1α in EBs (unpublished data). Our data support a notion that acute hypoxia induces Bnip3 expression mainly through HIF-1, whereas chronic hypoxia selectively stabilizes HIF-2α, which joins with HIF-1β in the nucleus and transactivates Bnip3 transcription.

Mitochondria have been suggested to play a key role in sensing changes of oxygen concentrations in cells and tissues (Brunelle et al., 2005; Guzy et al., 2005). AIF is a flavoprotein that is essential for maintaining the structural and functional integrity of mitochondrial complexes I and III (Vahsen et al., 2004). Inactivation of AIF in ES cells reduces the content of complexes I and III and suppresses oxidative phosphorylation. However, it is unknown whether AIF participates in HIF regulation. In this study, we observed a significant reduction of HIF-2α in the absence of AIF. Treatment of normal EBs with the complex I inhibitor rotenone also destabilizes HIF-2α. The reduced HIF-2α protein expression likely results from inhibition of ROS production in the core cells because increased ROS production is detected in the interior of $AIF^{y/+}$ but not $AIF^{y/-}$ EBs, the ROS scavenger EUK134 reduces HIF-2α in

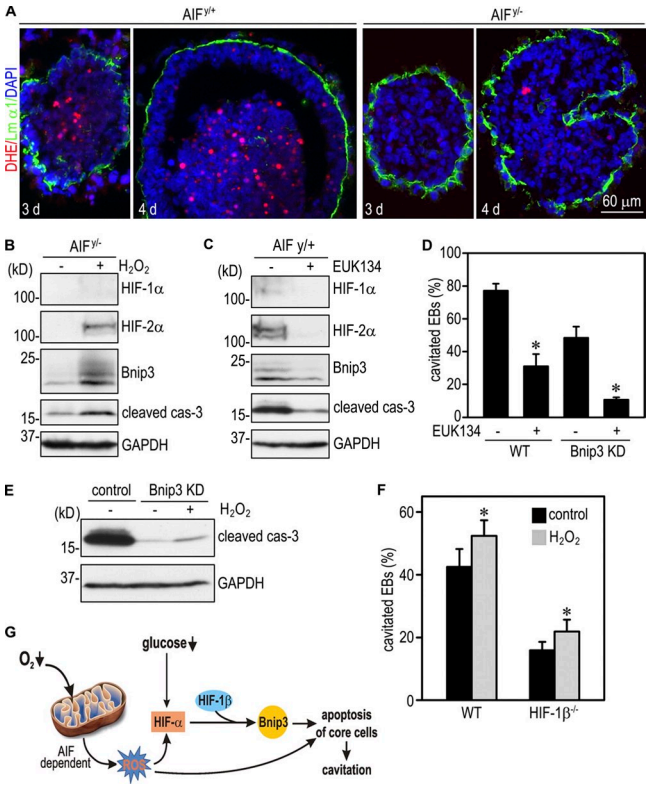

Figure 7. **ROS mediate AIF-dependent HIF-α stabilization, Bnip3 elevation, apoptosis, and cavitation.** (A) 3- and 4-d EBs were incubated with 60 nM DHE for 30 min and fixed in 3% PFA for 10 min. Basement membrane was stained with anti–laminin α1 antibody (Lm α1). DHE strongly labeled the centrally located cells in $AIF^{y/+}$ EBs, whereas DHE fluorescence was much weaker in $AIF^{y/-}$ EBs. (B) 2-d $AIF^{y/-}$ EBs were incubated with or without 0.1 mM H_2O_2 for 24 h and harvested for immunoblot analysis. H_2O_2 treatment led to a marked increase of HIF-2α, Bnip3, and cleaved caspase-3 (cas-3). GAPDH, glyceraldehyde 3-phosphate dehydrogenase. (C) 2-d $AIF^{y/+}$ EBs were treated with or without 2 μM EUK134 for 24 h. Immunoblots show that EUK134 treatment reduced the expression of HIF-1α, HIF-2α, Bnip3, and cleaved caspase-3. (D) 2-d wild-type (WT) and Bnip3 knockdown (KD) EBs were cultured with or without 2 μM EUK134 for an additional 5 d. EB cavitation was quantitated by phase microscopy. Cavitation of normal EBs was inhibited by EUK134 treatment. The cavitation efficiency was lower in Bnip3 knockdown EBs and was further reduced by EUK134 treatment. $n = 6$ independent experiments with a total of 634–753 EBs for each group. Error bars represent the mean ± SD. *, $P < 0.01$ versus EUK134 untreated group. (E) 2-d control and Bnip3 knockdown EBs were incubated with or without 0.1 mM H_2O_2 for 24 h and analyzed by immunoblotting for cleaved caspase-3. Bnip3 silencing markedly reduced cleaved caspase-3, whereas H_2O_2 treatment slightly increased its level. (F) 1-d EBs were treated with or without 0.1 mM H_2O_2 for 3 d. H_2O_2 treatment slightly increased the cavitation efficiency of both wild-type and $HIF\text{-}1\beta^{-/-}$ EBs. $n = 9$ independent experiments with a total of 909–1,004 EBs counted for each group. Error bars represent the mean ± SD. *, $P < 0.01$ versus control. (G) A model for EB cavitation. Hypoxia increases ROS production by mitochondria of the core cells in an AIF-dependent manner. Increased ROS and reduced glucose availability lead to HIF-2α stabilization and subsequent transactivation of Bnip3 expression. In turn, Bnip3 induces apoptosis of the core cells and cavitation. ROS can additionally trigger apoptosis independent of Bnip3.

$AIF^{y/+}$ EBs, and H_2O_2 increases HIF-2α in $AIF^{y/-}$ EBs. In addition, we have demonstrated that AIF not only cooperates with Bnip3 to induce apoptosis and cavitation but also regulates Bnip3 expression through HIFs. The latter is supported by the fact that ablation of AIF in EBs inhibits Bnip3 expression, whereas stable transfection of $AIF^{y/-}$ EBs with constitutively

active HIF-2α or HIF-1α restores Bnip3 expression. In all of these circumstances, the level of Bnip3 closely correlates with caspase-3 activation. Collectively, our results suggest a new mechanism of apoptosis induced by mitochondrial AIF under hypoxia. It is mediated through ROS production, HIF stabilization, and Bnip3 up-regulation. ROS produced in mitochondria could also induce apoptosis independent of Bnip3 (Simon et al., 2000). This is in line with our findings that the ROS scavenger EUK134 further inhibits cavitation in Bnip3 knockdown EBs, whereas H_2O_2 treatment slightly increases the cavitation efficiency of HIF-1$\beta^{-/-}$ EBs. Although AIF has been shown to directly induce nuclear condensation and chromatinolysis (Susin et al., 1999), we could not detect nuclear translocation of AIF even in the apoptotic cells in the EB interior.

In addition to hypoxia, the core cells of EBs are subject to limited glucose and increased lactic acid. We did not observe any effect of lactic acidosis on Bnip3 expression, although acidosis has been suggested to stabilize Bnip3 and increase its association with mitochondria (Kubasiak et al., 2002). Previous studies have shown that glucose deprivation can stabilize HIF-α through the AMP-activated protein kinase and mammalian target of rapamycin pathway (Hudson et al., 2002; Lee et al., 2003). In mouse ES cells, reduction in glucose levels in the culture medium causes apoptosis, and this is prevented by genetic ablation of HIF-2α, suggesting that HIF-2α–activated gene transcription inhibits hypoglycemia-induced apoptosis (Brusselmans et al., 2001). In this study, we show that the reduced glucose concentration up-regulates Bnip3 expression, which is mediated by HIFs, as inactivation of HIF-1β abolishes the Bnip3 up-regulation. Therefore, our data provide a mechanistic insight into hypoglycemia-induced apoptosis.

The mechanisms whereby Bnip3 induces apoptosis are incompletely understood. It is suggested that Bnip3 triggers apoptosis by inserting into the outer mitochondrial membrane through its C-terminal transmembrane domain (Chen et al., 1999; Kim et al., 2002; Regula et al., 2002). It opens the permeability transition pore and leads to loss of mitochondrial membrane potential. In cardiomyocytes, hypoxia-induced Bnip3 expression caused the opening of the permeability transition pore and DNA fragmentation, a hallmark of apoptotic cell death. However, the Bnip3-dependent apoptosis was not attenuated by caspase inhibition, suggesting that it is caspase independent (Kubasiak et al., 2002). Similarly, in neurons, Bnip3 has been shown to induce endonuclease G release from mitochondria and its translocation to the nucleus, where it cleaves DNA (Zhang et al., 2007). In fibroblasts, overexpression of Bnip3 caused loss of mitochondrial transmembrane potential, release of cytochrome C, and apoptosis, although caspase activation was not assessed (Kubli et al., 2007). In the present study, we show that apoptosis of the core cells during EB cavitation is associated with mitochondrial cytochrome C release and caspase-3 activation, both of which are inhibited by shRNA-mediated silencing of Bnip3. Altogether, these findings suggest that Bnip3 can induce apoptosis in both a caspase-dependent and -independent manner based on cell types studied.

Materials and methods

Culturing of ES cell and EBs

The ES cell lines used for this study were wild-type R1, HIF-1$\alpha^{-/-}$, HIF-2$\alpha^{-/-}$, HIF-1$\beta^{-/-}$, AIF$^{y/+}$, and AIF$^{y/-}$ ES cells (Maltepe et al., 1997; Carmeliet et al., 1998; Brusselmans et al., 2001; Joza et al., 2001). All the ES cells were cultured on mitomycin C–treated STO cells. EB differentiation was initiated from ES cell aggregates in suspension culture, as previously described (Li and Yurchenco, 2006). In brief, subconfluent ES cells were dispersed into small aggregates containing 20–30 cells with 0.05% trypsin/0.53 mM EDTA. Cells were collected into 15-ml conical tubes. Large ES cell aggregates and STO feeder cells were selectively removed by sedimentation under gravity. ES cell aggregates were cultured in nonadherent bacteriological Petri dishes in DME medium containing 15% FCS without leukemia inhibitory factor (Millipore).

Antibodies and cDNA constructs

pAbs to Bnip3, cleaved caspase-3, cytochrome C, and HIF-1β were purchased from Cell Signaling Technology. Perlecan mAb was purchased from Santa Cruz Biotechnology, Inc. Actin pAb was purchased from Sigma-Aldrich. HIF-1α and HIF-2α pAbs were purchased from Novus Biologicals. Bim pAb was purchased from Epitomics, Inc. AIF pAb was purchased from BD. Mitochondrial complex V mAb was purchased from Invitrogen. LC3 pAb was provided by M. Sakai (National Institute of Genetics, Shizuoka, Japan). MUPP1 pAb was provided by M. Adachi (Kyoto University, Kyoto, Japan). Cy3-, Cy5-, and HRP-conjugated secondary antibodies were purchased from Jackson ImmunoResearch Laboratories, Inc. Alexa Fluor 488–conjugated secondary antibodies were purchased from Invitrogen.

Four pGFP-V-RS–based shRNA vectors targeting to mouse Bnip3 and four pRFP-V-RS–based vectors targeting to Bim together with scrambled controls were purchased from OriGene. The effective sequence for Bnip3 is 5′-GGAGCAGCGTTCCAGCCTCCGTCTCTATT-3′ and for Bim is 5′-GAATGAGTTCGAGCGGCAGAGGTTCTGTT-3′. Mouse Bnip3 cDNA was amplified from 3-d normal EBs and cloned to the pCXN2-flag-IRES-GFP vector. The construct was confirmed by DNA sequencing. Mutant human HIF-1α PP and HIF-2α PPN in the pBabe-puro vector were obtained from Addgene (Yan et al., 2007).

Stable transfection of ES cells

For stable expression of Bnip3 or Bim shRNAs, normal ES cells were transfected with the shRNA vectors using Lipofectamine 2000 reagent (Invitrogen). Stable ES cell clones were selected with 2 µg/ml puromycin. For silencing of both Bnip3 and Bim, stable Bnip3 knockdown cell lines were transfected with the effective Bim shRNA, and double knockdown ES cell clones were selected based on the expression of both GFP and RFP. Similarly, pCXN2-Bnip3, pBabe–HIF-1α PP, pBabe–HIF-2α PPN, or the empty vector was introduced into ES cells using Lipofectamine 2000, and stable cell lines were selected based on either GFP fluorescence or puromycin resistance.

Gene expression profiling and RT-PCR

Total RNA was isolated from 2-, 3-, and 5-d normal EBs with TRIZOL reagent (Invitrogen) and was reverse transcribed to cRNA. Fragmented cRNAs were hybridized to mouse genome 430 2.0 microarray chips (Affymetrix). Hybridization data were analyzed by MAS software (v5.0; Affymetrix). For RT-PCR analysis, total RNA was reverse transcribed to cDNA. The PCR primers for mouse Bnip3 are 5′-TGAATCTGGACGAAGTAGCTCC-3′ (forward) and 5′-CAGACGCCTTCCAATGTAGATC-3′ (reverse). The primers for mouse Bim are 5′-GCCAAGCAACCTTCTGATG-3′ (forward) and 5′-CCAGACGGAAGATAAAGCG-3′ (reverse). 18S RNA served as a loading control.

Immunofluorescence

EB processing and immunostaining were performed as previously described (Li and Yurchenco, 2006). In brief, EBs were collected into 15-ml conical tubes and allowed to sediment by gravity. After washing in PBS, the EBs were fixed for 15 min with 3% PFA in PBS and then incubated in 7.5% sucrose-PBS for 3 h at room temperature. The EBs were embedded in optimal cutting temperature compound (Tissue-Tek; Miles Inc.), and 4-µm-thick cryosections were prepared on a cryostat (Leica). Alexa Fluor 488–, Cy3-, and Cy5-conjugated antibodies were used as secondary reagents. Nuclei were counterstained with DAPI. Slides were examined with an inverted fluorescence microscope (Eclipse TE2000; Nikon) and an oil immersion objective (40×, 1.30 NA, Plan Fluor; Nikon). Live-phase microscopy was performed at room temperature using a dry, extra-long

working-distance objective (20×, 0.45 NA, Plan Fluor; Nikon). Digital images were acquired with a cooled charge-coupled device camera (ORCA-03; Hamamatsu Photonics) controlled by IPLab software (Scanalytics). Cropping and rotation of images were performed with Photoshop CS4 (Adobe).

Immunoblotting and immunoprecipitation

EBs were collected by settling by gravity, washed once in PBS, and lysed in radioimmunoprecipitation assay (RIPA) buffer (50 mM Tris, pH 7.4, 150 mM NaCl, 1 mM EDTA, 1% NP-40, and 0.25% sodium deoxycholate) or SDS lysis buffer (50 mM Tris, pH 7.4, and 1% SDS) containing protease and phosphatase inhibitor cocktails. Immunoblottings were performed as previously described (Li et al., 2002). For immunoprecipitation, EBs were briefly lysed in RIPA buffer without sodium deoxycholate. After centrifugation, the pellet was washed and lysed in SDS lysis buffer. The nuclear lysates were then diluted with 10× RIPA buffer and immunoprecipitated using anti–HIF-2α antibody. Immunoblotting was followed using anti–HIF-1β antibody to determine HIF-2α binding to HIF-1β. Preparation of cytosolic and mitochondrial fractions was performed as previously described (Frezza et al., 2007). In brief, EBs were washed three times with NKM buffer (1 mM Tris-HCl, pH 7.4, 130 mM NaCl, 5 mM KCl, and 7.5 mM $MgCl_2$) and homogenized in homogenization buffer (10 mM Tris-HCl, pH 6.7, 10 mM KCl, 0.15 mM $MgCl_2$, 1 mM DTT, and protease inhibitor cocktail). Unbroken cells, nuclei, and large debris were removed by centrifugation at 1,200 *g* for 5 min. The mitochondria were pelleted by centrifugation at 7,000 *g* for 10 min and washed twice with mitochondria suspension buffer (10 mM Tris-HCl, pH 6.7, 0.15 mM $MgCl_2$, 250 mM sucrose, 1 mM DTT, and protease inhibitor cocktail). The mitochondria were lysed with RIPA buffer for immunoblotting.

ChIP assay

ChIP assay was performed using a ChIP assay kit (Millipore) as per the manufacturer's instruction. The PCR primers for the HIF-2α binding sequence in the Bnip3 promoter are 5′-CCGGTCCACTTCTGCATTAGACC-3′ and 5′-TGCGCCGCTCAGTTCTGAGG-3′. The primers for the HIF-2α binding sequence in the CITED2 promoter are 5′-TATTATTATCACCGCCTATTGC-3′ and 5′-AAGAAATTCGAGGGCTGAG-3′.

Statistical analysis

The percentages of EB cavitation were converted to arcsin values, and one-way analysis of variance was performed using SigmaStat 3.5. The immunoblot densitometry data were analyzed using Student's *t* test. All error bars represent the mean ± SD. The immunoblots shown are representatives of three experimental repeats, except for the time-course studies which are shown as a single representative experiment out of two repeats.

Online supplemental material

Fig. S1 shows the expression of HIF-1 and HIF-2 target genes during EB differentiation, as analyzed by global mRNA profiling. Fig. S2 shows the spatial expression of Bim in differentiating EBs and an E5.0 mouse embryo. It also depicts the effect of Bim knockdown and Bim/Bnip3 double knockdown on EB cavitation. Fig. S3 shows the expression of AIF during EB differentiation under hypoxia or in the absence of HIF-1α, HIF-2α, or HIF-1β. Fig. S4 shows the expression of Bnip3 in response to high- and low-glucose concentrations. Online supplemental material is available at http://www.jcb.org/cgi/content/full/jcb.201111063/DC1.

This work was supported by a grant from the National Institutes of Health (R01GM081674) to S. Li.

All authors declare no conflict of interest.

Submitted: 11 November 2011
Accepted: 7 June 2012

References

Arteel, G.E., R.G. Thurman, J.M. Yates, and J.A. Raleigh. 1995. Evidence that hypoxia markers detect oxygen gradients in liver: Pimonidazole and retrograde perfusion of rat liver. *Br. J. Cancer*. 72:889–895. http://dx.doi.org/10.1038/bjc.1995.429

Brown, D., B.D. Yu, N. Joza, P. Bénit, J. Meneses, M. Firpo, P. Rustin, J.M. Penninger, and G.R. Martin. 2006. Loss of Aif function causes cell death in the mouse embryo, but the temporal progression of patterning is normal. *Proc. Natl. Acad. Sci. USA*. 103:9918–9923. http://dx.doi.org/10.1073/pnas.0603950103

Bruick, R.K. 2000. Expression of the gene encoding the proapoptotic Nip3 protein is induced by hypoxia. *Proc. Natl. Acad. Sci. USA*. 97:9082–9087. http://dx.doi.org/10.1073/pnas.97.16.9082

Brunelle, J.K., E.L. Bell, N.M. Quesada, K. Vercauteren, V. Tiranti, M. Zeviani, R.C. Scarpulla, and N.S. Chandel. 2005. Oxygen sensing requires mitochondrial ROS but not oxidative phosphorylation. *Cell Metab.* 1:409–414. http://dx.doi.org/10.1016/j.cmet.2005.05.002

Brusselmans, K., F. Bono, P. Maxwell, Y. Dor, M. Dewerchin, D. Collen, J.M. Herbert, and P. Carmeliet. 2001. Hypoxia-inducible factor-2alpha (HIF-2alpha) is involved in the apoptotic response to hypoglycemia but not to hypoxia. *J. Biol. Chem.* 276:39192–39196. http://dx.doi.org/10.1074/jbc.C100428200

Carmeliet, P., Y. Dor, J.M. Herbert, D. Fukumura, K. Brusselmans, M. Dewerchin, M. Neeman, F. Bono, R. Abramovitch, P. Maxwell, et al. 1998. Role of HIF-1alpha in hypoxia-mediated apoptosis, cell proliferation and tumour angiogenesis. *Nature*. 394:485–490. http://dx.doi.org/10.1038/28867

Chen, G., J. Cizeau, C. Vande Velde, J.H. Park, G. Bozek, J. Bolton, L. Shi, D. Dubik, and A. Greenberg. 1999. Nix and Nip3 form a subfamily of pro-apoptotic mitochondrial proteins. *J. Biol. Chem.* 274:7–10. http://dx.doi.org/10.1074/jbc.274.1.7

Chinnadurai, G., S. Vijayalingam, and S.B. Gibson. 2008. BNIP3 subfamily BH3-only proteins: Mitochondrial stress sensors in normal and pathological functions. *Oncogene*. 27(Suppl 1):S114–S127. http://dx.doi.org/10.1038/onc.2009.49

Coucouvanis, E., and G.R. Martin. 1995. Signals for death and survival: A two-step mechanism for cavitation in the vertebrate embryo. *Cell*. 83:279–287. http://dx.doi.org/10.1016/0092-8674(95)90169-8

Coucouvanis, E., and G.R. Martin. 1999. BMP signaling plays a role in visceral endoderm differentiation and cavitation in the early mouse embryo. *Development*. 126:535–546.

Daido, S., T. Kanzawa, A. Yamamoto, H. Takeuchi, Y. Kondo, and S. Kondo. 2004. Pivotal role of the cell death factor BNIP3 in ceramide-induced autophagic cell death in malignant glioma cells. *Cancer Res.* 64:4286–4293. http://dx.doi.org/10.1158/0008-5472.CAN-03-3084

Datta, A., D.M. Bryant, and K.E. Mostov. 2011. Molecular regulation of lumen morphogenesis. *Curr. Biol.* 21:R126–R136. http://dx.doi.org/10.1016/j.cub.2010.12.003

Debnath, J., K.R. Mills, N.L. Collins, M.J. Reginato, S.K. Muthuswamy, and J.S. Brugge. 2002. The role of apoptosis in creating and maintaining luminal space within normal and oncogene-expressing mammary acini. *Cell*. 111:29–40. http://dx.doi.org/10.1016/S0092-8674(02)01001-2

Diwan, A., M. Krenz, F.M. Syed, J. Wansapura, X. Ren, A.G. Koesters, H. Li, L.A. Kirshenbaum, H.S. Hahn, J. Robbins, et al. 2007. Inhibition of ischemic cardiomyocyte apoptosis through targeted ablation of Bnip3 restrains postinfarction remodeling in mice. *J. Clin. Invest.* 117:2825–2833. http://dx.doi.org/10.1172/JCI32490

Frezza, C., S. Cipolat, and L. Scorrano. 2007. Organelle isolation: Functional mitochondria from mouse liver, muscle and cultured fibroblasts. *Nat. Protoc.* 2:287–295. http://dx.doi.org/10.1038/nprot.2006.478

Green, D.R., and J.C. Reed. 1998. Mitochondria and apoptosis. *Science*. 281:1309–1312. http://dx.doi.org/10.1126/science.281.5381.1309

Guzy, R.D., B. Hoyos, E. Robin, H. Chen, L. Liu, K.D. Mansfield, M.C. Simon, U. Hammerling, and P.T. Schumacker. 2005. Mitochondrial complex III is required for hypoxia-induced ROS production and cellular oxygen sensing. *Cell Metab.* 1:401–408. http://dx.doi.org/10.1016/j.cmet.2005.05.001

He, X., J. Liu, Y. Qi, C. Brakebusch, A. Chrostek-Grashoff, D. Edgar, P.D. Yurchenco, S.A. Corbett, S.F. Lowry, A.M. Graham, et al. 2010. Rac1 is essential for basement membrane-dependent epiblast survival. *Mol. Cell. Biol.* 30:3569–3581. http://dx.doi.org/10.1128/MCB.01366-09

Hogan, B.L., and P.A. Kolodziej. 2002. Organogenesis: Molecular mechanisms of tubulogenesis. *Nat. Rev. Genet.* 3:513–523. http://dx.doi.org/10.1038/nrg840

Holmquist-Mengelbier, L., E. Fredlund, T. Löfstedt, R. Noguera, S. Navarro, H. Nilsson, A. Pietras, J. Vallon-Christersson, A. Borg, K. Gradin, et al. 2006. Recruitment of HIF-1alpha and HIF-2alpha to common target genes is differentially regulated in neuroblastoma: HIF-2alpha promotes an aggressive phenotype. *Cancer Cell*. 10:413–423. http://dx.doi.org/10.1016/j.ccr.2006.08.026

Hu, C.J., L.Y. Wang, L.A. Chodosh, B. Keith, and M.C. Simon. 2003. Differential roles of hypoxia-inducible factor 1alpha (HIF-1alpha) and HIF-2alpha in hypoxic gene regulation. *Mol. Cell. Biol.* 23:9361–9374. http://dx.doi.org/10.1128/MCB.23.24.9361-9374.2003

Hudson, C.C., M. Liu, G.G. Chiang, D.M. Otterness, D.C. Loomis, F. Kaper, A.J. Giaccia, and R.T. Abraham. 2002. Regulation of hypoxia-inducible factor 1alpha expression and function by the mammalian target of rapamycin. *Mol. Cell. Biol.* 22:7004–7014. http://dx.doi.org/10.1128/MCB.22.20.7004-7014.2002

Joza, N., S.A. Susin, E. Daugas, W.L. Stanford, S.K. Cho, C.Y. Li, T. Sasaki, A.J. Elia, H.Y. Cheng, L. Ravagnan, et al. 2001. Essential role of the mitochondrial apoptosis-inducing factor in programmed cell death. *Nature*. 410:549–554. http://dx.doi.org/10.1038/35069004

Joza, N., G.Y. Oudit, D. Brown, P. Bénit, Z. Kassiri, N. Vahsen, L. Benoit, M.M. Patel, K. Nowikovsky, A. Vassault, et al. 2005. Muscle-specific loss of apoptosis-inducing factor leads to mitochondrial dysfunction, skeletal muscle atrophy, and dilated cardiomyopathy. *Mol. Cell. Biol.* 25:10261–10272. http://dx.doi.org/10.1128/MCB.25.23.10261-10272.2005

Kim, J.Y., J.J. Cho, J. Ha, and J.H. Park. 2002. The carboxy terminal C-tail of BNip3 is crucial in induction of mitochondrial permeability transition in isolated mitochondria. *Arch. Biochem. Biophys.* 398:147–152. http://dx.doi.org/10.1006/abbi.2001.2673

Kubasiak, L.A., O.M. Hernandez, N.H. Bishopric, and K.A. Webster. 2002. Hypoxia and acidosis activate cardiac myocyte death through the Bcl-2 family protein BNIP3. *Proc. Natl. Acad. Sci. USA*. 99:12825–12830. http://dx.doi.org/10.1073/pnas.202474099

Kubli, D.A., J.E. Ycaza, and A.B. Gustafsson. 2007. Bnip3 mediates mitochondrial dysfunction and cell death through Bax and Bak. *Biochem. J.* 405:407–415. http://dx.doi.org/10.1042/BJ20070319

Lee, M., J.T. Hwang, H.J. Lee, S.N. Jung, I. Kang, S.G. Chi, S.S. Kim, and J. Ha. 2003. AMP-activated protein kinase activity is critical for hypoxia-inducible factor-1 transcriptional activity and its target gene expression under hypoxic conditions in DU145 cells. *J. Biol. Chem.* 278:39653–39661. http://dx.doi.org/10.1074/jbc.M306104200

Li, S., and P.D. Yurchenco. 2006. Matrix assembly, cell polarization, and cell survival: Analysis of peri-implantation development with cultured embryonic stem cells. *Methods Mol. Biol.* 329:113–125.

Li, S., D. Harrison, S. Carbonetto, R. Fassler, N. Smyth, D. Edgar, and P.D. Yurchenco. 2002. Matrix assembly, regulation, and survival functions of laminin and its receptors in embryonic stem cell differentiation. *J. Cell Biol.* 157:1279–1290. http://dx.doi.org/10.1083/jcb.200203073

Li, S., D. Edgar, R. Fässler, W. Wadsworth, and P.D. Yurchenco. 2003. The role of laminin in embryonic cell polarization and tissue organization. *Dev. Cell*. 4:613–624. http://dx.doi.org/10.1016/S1534-5807(03)00128-X

Liu, J., X. He, S.A. Corbett, S.F. Lowry, A.M. Graham, R. Fässler, and S. Li. 2009. Integrins are required for the differentiation of visceral endoderm. *J. Cell Sci.* 122:233–242. http://dx.doi.org/10.1242/jcs.037663

Mailleux, A.A., M. Overholtzer, T. Schmelzle, P. Bouillet, A. Strasser, and J.S. Brugge. 2007. BIM regulates apoptosis during mammary ductal morphogenesis, and its absence reveals alternative cell death mechanisms. *Dev. Cell*. 12:221–234. http://dx.doi.org/10.1016/j.devcel.2006.12.003

Majmundar, A.J., W.J. Wong, and M.C. Simon. 2010. Hypoxia-inducible factors and the response to hypoxic stress. *Mol. Cell*. 40:294–309. http://dx.doi.org/10.1016/j.molcel.2010.09.022

Maltepe, E., J.V. Schmidt, D. Baunoch, C.A. Bradfield, and M.C. Simon. 1997. Abnormal angiogenesis and responses to glucose and oxygen deprivation in mice lacking the protein ARNT. *Nature*. 386:403–407. http://dx.doi.org/10.1038/386403a0

Meyer, T.N., C. Schwesinger, K.T. Bush, R.O. Stuart, D.W. Rose, M.M. Shah, D.A. Vaughn, D.L. Steer, and S.K. Nigam. 2004. Spatiotemporal regulation of morphogenetic molecules during in vitro branching of the isolated ureteric bud: Toward a model of branching through budding in the developing kidney. *Dev. Biol.* 275:44–67. http://dx.doi.org/10.1016/j.ydbio.2004.07.022

Mizushima, N., and T. Yoshimori. 2007. How to interpret LC3 immunoblotting. *Autophagy*. 3:542–545.

Modjtahedi, N., F. Giordanetto, F. Madeo, and G. Kroemer. 2006. Apoptosis-inducing factor: Vital and lethal. *Trends Cell Biol.* 16:264–272. http://dx.doi.org/10.1016/j.tcb.2006.03.008

Murray, P., and D. Edgar. 2000. Regulation of programmed cell death by basement membranes in embryonic development. *J. Cell Biol.* 150:1215–1221. http://dx.doi.org/10.1083/jcb.150.5.1215

Pradhan, S., C. Liu, C. Zhang, X. Jia, M.C. Farach-Carson, and R.L. Witt. 2010. Lumen formation in three-dimensional cultures of salivary acinar cells. *Otolaryngol. Head Neck Surg.* 142:191–195. http://dx.doi.org/10.1016/j.otohns.2009.10.039

Qu, X., Z. Zou, Q. Sun, K. Luby-Phelps, P. Cheng, R.N. Hogan, C. Gilpin, and B. Levine. 2007. Autophagy gene-dependent clearance of apoptotic cells during embryonic development. *Cell*. 128:931–946. http://dx.doi.org/10.1016/j.cell.2006.12.044

Quinsay, M.N., Y. Lee, S. Rikka, M.R. Sayen, J.D. Molkentin, R.A. Gottlieb, and A.B. Gustafsson. 2010. Bnip3 mediates permeabilization of mitochondria and release of cytochrome c via a novel mechanism. *J. Mol. Cell. Cardiol.* 48:1146–1156. http://dx.doi.org/10.1016/j.yjmcc.2009.12.004

Reginato, M.J., K.R. Mills, E.B. Becker, D.K. Lynch, A. Bonni, S.K. Muthuswamy, and J.S. Brugge. 2005. Bim regulation of lumen formation in cultured mammary epithelial acini is targeted by oncogenes. *Mol. Cell. Biol.* 25:4591–4601. http://dx.doi.org/10.1128/MCB.25.11.4591-4601.2005

Regula, K.M., K. Ens, and L.A. Kirshenbaum. 2002. Inducible expression of BNIP3 provokes mitochondrial defects and hypoxia-mediated cell death of ventricular myocytes. *Circ. Res.* 91:226–231. http://dx.doi.org/10.1161/01.RES.0000029232.42227.16

Simon, H.U., A. Haj-Yehia, and F. Levi-Schaffer. 2000. Role of reactive oxygen species (ROS) in apoptosis induction. *Apoptosis*. 5:415–418. http://dx.doi.org/10.1023/A:1009616228304

Susin, S.A., H.K. Lorenzo, N. Zamzami, I. Marzo, B.E. Snow, G.M. Brothers, J. Mangion, E. Jacotot, P. Costantini, M. Loeffler, et al. 1999. Molecular characterization of mitochondrial apoptosis-inducing factor. *Nature*. 397:441–446. http://dx.doi.org/10.1038/17135

Vahsen, N., C. Candé, J.J. Brière, P. Bénit, N. Joza, N. Larochette, P.G. Mastroberardino, M.O. Pequignot, N. Casares, V. Lazar, et al. 2004. AIF deficiency compromises oxidative phosphorylation. *EMBO J.* 23:4679–4689. http://dx.doi.org/10.1038/sj.emboj.7600461

Varghese, A.J., S. Gulyas, and J.K. Mohindra. 1976. Hypoxia-dependent reduction of 1-(2-nitro-1-imidazolyl)-3-methoxy-2-propanol by Chinese hamster ovary cells and KHT tumor cells in vitro and in vivo. *Cancer Res.* 36:3761–3765.

Wang, V., D.A. Davis, M. Haque, L.E. Huang, and R. Yarchoan. 2005. Differential gene up-regulation by hypoxia-inducible factor-1alpha and hypoxia-inducible factor-2alpha in HEK293T cells. *Cancer Res.* 65:3299–3306.

Wells, K.L., and N. Patel. 2010. Lumen formation in salivary gland development. *Front Oral Biol*. 14:78–89. http://dx.doi.org/10.1159/000313708

Yan, Q., S. Bartz, M. Mao, L. Li, and W.G. Kaelin Jr. 2007. The hypoxia-inducible factor 2alpha N-terminal and C-terminal transactivation domains cooperate to promote renal tumorigenesis in vivo. *Mol. Cell. Biol.* 27:2092–2102. http://dx.doi.org/10.1128/MCB.01514-06

Zhang, J., and P.A. Ney. 2009. Role of BNIP3 and NIX in cell death, autophagy, and mitophagy. *Cell Death Differ.* 16:939–946. http://dx.doi.org/10.1038/cdd.2009.16

Zhang, Z., X. Yang, S. Zhang, X. Ma, and J. Kong. 2007. BNIP3 upregulation and EndoG translocation in delayed neuronal death in stroke and in hypoxia. *Stroke*. 38:1606–1613. http://dx.doi.org/10.1161/STROKEAHA.106.475129